DentalTouch: A Haptic Display with High Stiffness and Low Inertia*

Hongdong Zhang, Yuru Zhang, *Senior Member, IEEE*, Dangxiao Wang, *Senior Member, IEEE*, and Lei Lu

Abstract— **Designing haptic devices with both high stiffness and low inertia is challenging. In this paper, we propose a solution to overcome the difficulty. We present a new haptic device named DentalTouch for dental simulation. Combining parallel and serial mechanisms, the DentalTouch can render 3-dimentional forces and 6 degree-of-freedom (DOF) motions. We describe how to achieve high stiffness and low inertia in the DentalTouch by using co-actuation method recently developed by our group. We evaluate the stiffness and inertia performance of a DentalTouch prototype through analytical and experimental approaches. The results show that the combined structural and motor control stiffness of the prototype is within the range of 21-69 N/mm and the inertia ranges from 113 to 163 g in task workspace, which demonstrates that the DentalTouch has a potential to provide a high stiffness and low inertia.**

I. INTRODUCTION

Dental simulation has been putting forward great challenges to the design of haptic interfaces [1]. The simulation of hard teeth and light tools demands that haptic devices can render high stiffness and low inertia. As suggested by [2], stiffness higher than 24 N/mm is required to simulate hard contact. Meanwhile, the weight of the most dental tools is less than 10 g. Such requirement for simultaneous high stiffness and low inertial places a great challenge in the design of haptic devices.

Haptic displays can be classified into impedance devices and admittance devices. Impedance displays are usually highly back-drivable with low inertia and friction [3] [4]. Admittance displays are often highly geared, and are therefore non-back-drivable due to high inertia and friction [5] [6]. Existing impedance devices can have an unmasked inertia as low as 0.05 kg, thus are suitable for simulating low inertia environments, but have difficulty rendering stiff constraints. For example, notable Phantom devices have an unmasked inertia from 45 to 150 g, but their maximum stable stiffness is small, ranging from 1-3.5 N/mm [7]. On the other hand, admittance devices are able to render high stiffness and large force. But they typically have a minimum stable mass of 2-5 kg, thus are struggle to simulate free motion. Notable admittance haptic devices, Haptic master [5] has a high stable stiffness of 10-50 N/mm, but its minimum stable mass is 2 kg. Therefore, it is difficult for conventional impedance and admittance devices to achieve simultaneously high stiffness and low inertia.

Great efforts have been made to increase dynamic range of haptic devices. Zinn *et al*. [8] introduced a new actuation approach based on parallel actuation concept to overcome the limitation of traditional impedance devices. They used a high-power, high-torque actuator to provide the low frequency torques while a small, fast actuator to provide the high frequency torques. Experimental results showed that the approach was able to achieve a high stiffness of 57 N/mm for a 3-DOF prototype within a large workspace of 0.6 m^3.

Several researchers have investigated the use of brakes to achieve high impedance and thus improve stability. Different types of brakes were used [9-13]. It was found that some characteristics of the brakes, such as slow to actuate and nonlinear relationship between velocity and torque, limit the fidelity of the rendering. To improve the performance, Gosline and Hayward proposed to use eddy current brakes (ECBs) as linear, fast actuating, programmable viscous dampers for haptic rendering. However, the use of dampers in brakes leads to increase in the inertia and power consumption of the device [14]. Alternatively, the dissipative properties of a DC motor were taken as an advantage to realize programmable electrical damping [15].

Another concept to provide a convincingly hard surface is to use mechanical constraints. A typical example was Cobot, which used parallel linkage to build a 6-DOF device. Although controlled as an admittance device, the Cobot does not suffer from the high inertia, friction and backlash that normally exist in a highly geared admittance device. With the novel mechanical design, the Cobot had a structural stiffness ranging from 20-400 N/mm. A further variation on mechanical constraints is dynamic physical constraints (DPC) proposed to emulate a virtual surface that is approximately concentric with the central pivot point [16]. The DPC concept can produce a realistic sensation of hard surface contact because of the real physical contact between the user and the DPC.

In the past decades, several dental simulators have been developed [17]. For most simulators, impedance haptic devices were used. An exception is the Simodont system (MOOG Inc.), which used a self-developed admittance haptic device [18]. However, no detailed quantitative information was found in the literature.

In this paper, we introduce DentalTouch, a 6-DOF admittance display. Our goal is to design and implement a novel haptic device that can simulate both high stiffness and low inertia required for dental simulation. To overcome the drawback of non-back drivability and large inertia of conventional admittance displays, we apply co-actuation concept [19] to make the DentalTouch back drivable and meanwhile have small mass comparable to that of impedance displays. In Section II we provide a detailed description of

mechanical design of the DentaTouch. In Section III we derive dynamic model of the DentalTouch and analyze the gravity and inertia. In Section IV we measure gravity and stiffness of the device. Finally we make conclusions in Section V.

II. DESCRIPTION OF DENTALTOUCH

A. Mechanism

The mechanism of the DentalTouch is a combination of a 3-DOF parallel and a 3-DOF serial mechanism as shown in Figure 1. The parallel mechanism consists of three limbs: two identical RSS limbs (R: revolute joint; S: spherical joint) and one 3R limb. The joints 3 and 4 of the 3R limb are in parallel, and the joint 5 is perpendicular to the joint 4 and their axes intersect at the point N as shown in Figure 1 (b). The serial mechanism has three revolute joints, the axes of which are perpendicular to each other and intersect at the point Q. The serial mechanism is connected to the moving platform m through the joint 6.

The parallel and serial mechanisms provide translational and rotational motion of the end-effector respectively. Three co-actuation modules [19] are applied at the joint 1, 2 and 3. Hence, the DentalTouch allows 6-DOF motion of the end-effector, and can render 3-dimentional force at the point Q.

The forward kinematics of the DentalTouch presented in [20] was used to calculate the displacement of Q when measuring the stiffness of the DentalTouch. The formulation of Jacobian matrix is briefly reviewed in the Appendix for the sake of clarity. The Jacobian matrix was used to analyze the effective gravity of the DentalTouch.

We defined the task workspace as a cube and computed it using a search algorithm with a resolution of 1 mm. The task workspace enclosed in the reachable workspace has a maximum length of 88 mm, which is large enough for simulating an oral cavity. Figure 5 (a) shows the task workspace relative to the base frame.
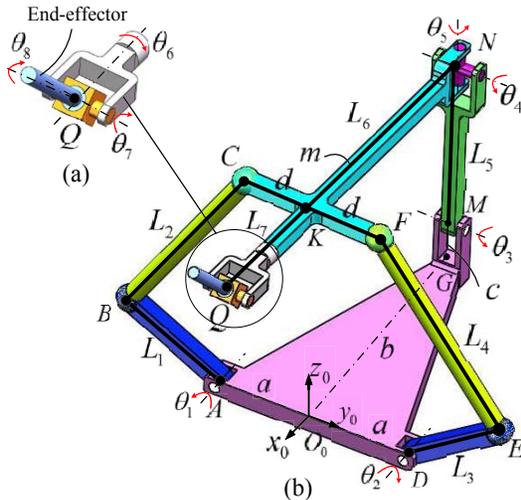
Fig. 1. The schematic diagram of the DentalTouch. (a) The 3R serial mechanism provides 3-DOF rotations. (b) The 6-DOF mechanism of the DentalTouch.
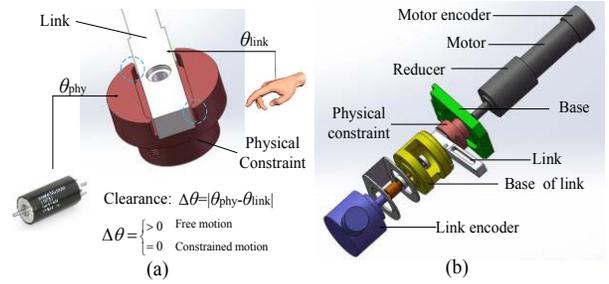
Fig. 2. Co-actuation module. (a) The principle of co-actuation. (b) Mechanical structure of the co-actuation module.

B. Actuation

To achieve high stiffness and low inertia, we apply co-actuation approach [19] to implement the first prototype of the DentalTouch. Figure 2 illustrates the principle of the co-actuation concept and the detailed structure of a co-actuation module. The co-actuation module consists of two parts: the input link and the physical constraint. A clearance is designed between the input link and the physical constraint which is actuated by a motor with a high-ratio gear reducer. Two optical encoders are respectively mounted on the shaft of the motor and the link to measure their positions. There are two control modes for the physical constraint: free motion and constraint motion. In free motion mode, the physical constraint follows the input link while keeping a distance from it. Therefore, the user would not feel the inertia and friction of the motor and the gear box, which results in a great reduction of perceived inertia and friction. In constraint motion, the physical constraint applies a reaction force to the input link by keeping a contact with it. The physical constraint can provide a power as high as necessary by using high gear ratio. Therefore, the user would feel a stiff constraint against his/her motion.

The control scheme of the DentalTouch is shown in Figure 3. Collision checking determines which control mode is selected. In the case of constraint motion, conventional admittance control algorithm can be adopted to render stiff objects. In the case of free motion, conventional motion control can be applied to make the physical constraint track the motion of the input link. As shown in Figure 3 (b), two
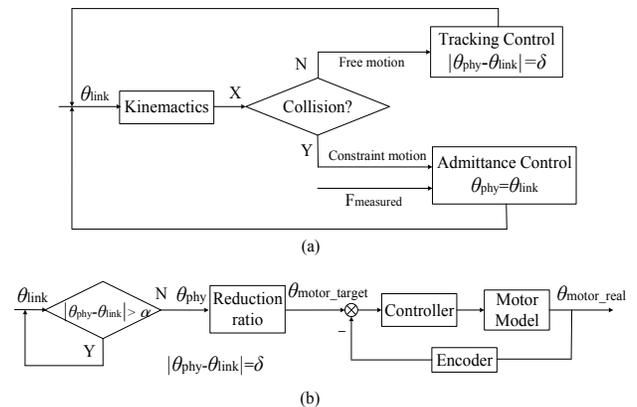
Fig. 3. Control scheme of the DentalTouch. (a) Switching between free motion and constraint motion modes according to collision checking. (b) Diagram of the tracking control in free motion.
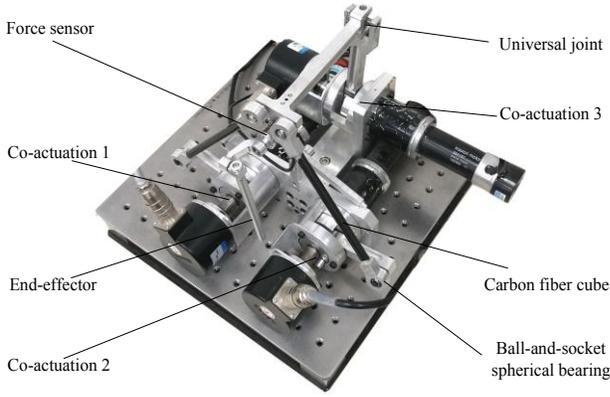
Fig. 4. The prototype of the DentalTouch.

parameters, α and δ, are introduced in the tracking control mode. α is used to ensure the transparency in free space. δ is defined to control the penetration depth between a virtual tool and a virtual wall. If the clearance between the physical constraint and the link is larger than α, the physical constraint stays in the current position. When the link is getting closer to the physical constraint, the motion control is triggered so that the physical constraint keeps a distance of δ with the link. The value of δ and α can be selected according to the requirements of simulated tasks.

Figure 4 shows the full assembly of the DentalTouch. The base joint of each limb is driven by a co-actuation module. Each co-actuation module consists of a 60 W brush DC motor (Maxon RE30) connected to a harmonic gear reducer (HarmonicDrive CSF11) with a reduction ratio of 50. The motor and link encoders have a resolution of 0.036° and 0.0049° respectively. In the implementation of spherical joints, the ball-and-socket spherical bearing was adopted for its simple and compact mechanical structure. Low friction of the ball bearing can be achieved by careful clearance design and appropriate lubrication. We designed the joints 4 and 5 in the 3R limb with a cross shaped shaft, which can achieve motion ranges larger than conventional universal joints. Because the links BC and EF transmit axial forces only, we design their structures with carbon fiber tubes to obtain a relatively high stiffness in the axial direction and low mass.

III. DYNAMICS

In this section, we model the dynamics of the DentalTouch and evaluate back-drive performance using effective gravity and inertia at the end-effector.

A. Effective Gravity

The dynamics of the DentalTouch in Cartesian space can be written in the general form

$$F = M_x(\Theta) \ddot{X} + V_x(\Theta, \dot{\Theta}) + G_x(\Theta) \qquad (1)$$

where the vector F is a force acting on the end-effector, X is the position vector of the reference point Q, $M_x(\Theta)$ is the inertia matrix, $V_x(\Theta, \dot{\Theta})$ is a vector related to velocities and $G_x(\Theta)$ is a vector related to gravity.

The effective gravity of the end-effector can be defined as:

$$G_e = G_x(\Theta)_3 \qquad (2)$$

where $G_x(\Theta)_3$ is the third element of the vector $G_x(\Theta)$. The expression of the effective gravity at the end-effector of the DentalTouch is presented in Appendix.

We calculated the effective gravity at the end-effector in the whole task workspace using Eq. (2). The maximum and minimum calculated effective gravities are approximately 1.13 N and 0.65 N respectively. The effective gravity of the current DentalTouch prototype is not as small as required for simulating light dental tools. Further reduction of the effective gravity is necessary. Conventional design methods such as static balancing [22-24] can be used for this purpose. An alternative approach is to decrease the gravity of mechanical elements through topological optimization.

B. Effective Inertia

In traditional haptic devices, the effective inertia is a function of both the link inertia as well as the reflected actuator inertia. However, the DentalTouch is an exception due to the decoupling of the actuator from the link in the co-actuation module. The inertia of the actuator along with its gear train is not reflected to the end-effector, thus results in an effective reduction in the inertia of the device.

The effective inertia at the end effector can be determined using the first item in Eq. (1). However, deducing the expression of $M_x(\Theta)$ is not efficient because of the dynamic complexity of the DentalTouch. Therefore we used Adams software to compute the effective inertia.

The symmetric inertia matrix $M_x(\Theta)$ at the end-effector can be formed as:

$$M_x(\Theta) = \begin{bmatrix} m_1 & m_2 & m_3 \\ m_2 & m_4 & m_5 \\ m_3 & m_5 & m_6 \end{bmatrix} \qquad (3)$$

The maximum effective inertia m_e at a given position can be calculated by:

$$m_e = \lambda_{\max}(M_x(\Theta)) \qquad (4)$$

where $\lambda_{\max}$ is the maximum eigenvalue of $M_x(\Theta)$.

In the Adams simulation, to eliminate the effect of $G_x(\Theta)$ and $V_x(\Theta, \dot{\Theta})$ in Eq. (1), the gravitational acceleration and the initial velocities were set to zero. As a result, Eq. (1) can be simplified as:

$$\begin{bmatrix} F_x \\ F_y \\ F_z \end{bmatrix} = \begin{bmatrix} m_1 & m_2 & m_3 \\ m_2 & m_4 & m_5 \\ m_3 & m_5 & m_6 \end{bmatrix} \begin{bmatrix} a_x \\ a_y \\ a_z \end{bmatrix} \qquad (5)$$

where the force and the acceleration vectors are written in the Cartesian coordinate system of the base frame.
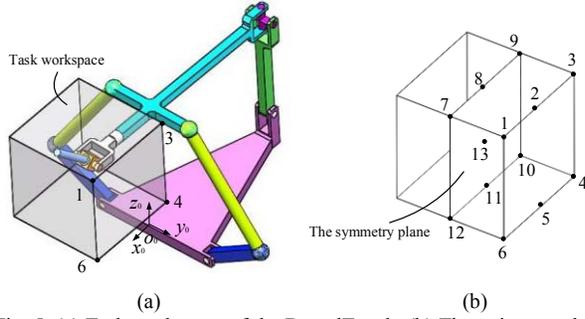
Fig. 5. (a) Task workspace of the DentalTouch. (b) The points at which the effective inertia was computed.

Fig. 6. Measured force and displacement at the point Q and the fitting result.

TABLE I. THE EFFECTIVE INERTIA AT GIVEN POINTS

Points	Effective Inertia (g)	Points	Effective Inertia (g)
1	162	8	114
2	118	9	114
3	116	10	154
4	163	11	121
5	123	12	113
6	118	13 Center of workspace	113
7	143		

To compute $M_x(\Theta)$ in Adams, the end-effector was first moved to a given position. A unit force along x_0 (F_x=1N; F_y=F_z=0) was then applied to Q. Measuring the accelerations a_x, a_y and a_z at the initial position, we obtained three equations with respect to m_i (i=1 to 6) by Eq. (5). Applying a second unit force along y_0 (F_x=F_z=0; F_y=1 N) and a third unit force along z_0 (F_x=F_y=0; F_z=1N) to Q, six more equations could be obtained following the same step above. It should be noted that only six of the nine obtained equations are linearly independent. Solving the six linearly independent equations for m_i (i=1 to 6), the inertia matrix $M_x(\Theta)$ were obtained. Upon obtaining the inertia matrix, the maximum effective inertia at this position can be obtained by Eq. (4).

Because the DentalTouch is symmetrical with respect to the x_0 axis, we selected some typical points in half of the task workspace to compute the effective inertia as shown in Figure 5 (b). Table I illustrated the results. It is noted that the effective inertia is larger at the boundary of the task workspace. The maximum effective inertia is approximately 163 g. Considering that the current prototype is not optimized in structural design, further reduction of the effective inertia would be possible.

IV. EXPERIMENTAL EVALUATION

In this section, we evaluate the performance of the DentalTouch in the aspect of stiffness and effective gravity at the end-effector by experimental method. We firstly measure the stiffness at points randomly selected in the task workspace. Then, we compare the theoretical results of effective gravity to the experimental results. Comparison demonstrates the accuracy of the theoretical model of effective gravity.
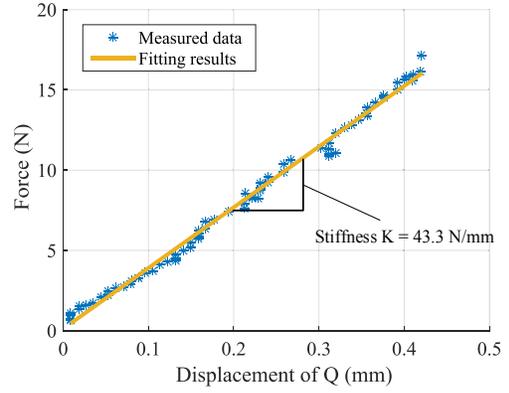
A. Stiffness experiment

In the experiment of stiffness measurement, the force, applied at the point Q, was measured using a six dimensional force-torque sensor (ATI Nano 17, ranges: F_x=F_y=50 N, F_z=70 N; resolutions: ΔF_x=ΔF_y=0.006 N, ΔF_z=0.003 N) while the end-effector position was determined using the forward kinematics of the device with measured joint angles of links.

We measured the stiffness at five points, which were selected randomly in the task workspace. For each point, we firstly calculated the base joint angles using the inverse kinematics of the DentalTouch. The calculated joint angles were then used as the target positions of the physical constraints of the co-actuation modules. The three motors of the modules were controlled to the target positions. A self-developed PID controller (Current loop: 24 kHz, velocity and position loops: 1 kHz) was used to control the motors. When the force applied to the end-effector along a given direction, e.g. the x_0 axis, was continuously increased, the displacement of the point Q in the same direction was recorded. The stiffness was estimated using the measured force and the displacement.

Figure 6 illustrates the relationship between the applied force and the displacement of the point Q at one of the five positions. The force was applied to the point Q in the direction of the unit vector (-0.96, 0.07, -0.27) in Cartesian coordinate system. From the measured data, the stiffness at this point was estimated to be 43.3 N/mm, which equals to the slope of the fitting result. Furthermore, the measured stiffness at the five points is within the range of 21-69 N/mm. It should be noted that the property of virtual environment was not involved in the measurement. Thus the estimated stiffness only reflects the stiffness performance of the mechanical structure and the motor control systems.

B. Gravity measurement

To evaluate the effective gravity and verify the theoretical model, we conducted experiments using the prototype of the DentalTouch. In the experiment, the effective gravity at the end-effector was measured using the ATI force sensor while the base joint angles were recorded to calculate the end-effector position using the forward kinematics. The

TABLE II. EXPERIMENTAL RESULTS OF EFFECTIVE GRAVITY

Position of measurement (x, y, z)	Results		
	Measured(N)	Theoretical(N)	Error
(54.5, 8.5, 134.5)	1.07	1.10	2.7%
(57.3, -19.3, 159.8)	1.01	1.04	2.9%
(19.3, -13.8, 127.2)	1.15	1.09	5.5%
(52.1, -0.6, 143.9)	1.02	1.08	5.6%
(-9.8, -49.9, 210.9)	1.08	1.06	1.9%

theoretical effective gravity was calculated using Eq. (8-A). Comparison between the experimental and theoretical results is illustrated in Table II. The maximum measured effective gravity is approximately 1.15 N and the maximum error between the experimental and theoretical results is about 5.6%.

V. CONCLUSION

We have proposed a new haptic device, DentalTouch, for dental simulation, which combines parallel and serial mechanisms to render 3-dimentional forces and 6-DOF motions. The co-actuation method proposed in [19] was adopted in a DentalTouch prototype to achieve high stiffness and low inertia. Advantages of using the co-actuation method include: 1) Reducing the inertia and power requirement of the device. This allows the motor response faster, thus improve the performance in simulating hard contact. 2) Dynamics of the physical constraints is independent from the device configuration. This allows the device performance more uniform across the workspace than without using the co-actuation. It should be noted that gravity compensation is difficult to implement in the co-actuation approach. Therefore, if the device mechanism is large and heavy, and motor power is required to compensate gravity, alternative approaches need to be considered.

Our preliminary experimental study on the stiffness and inertia performance of the device showed that the DentalTouch prototype has a high stiffness comparable to that of admittance haptic devices while having a relative low effective inertia comparable to that of impedance haptic devices. The experimental and simulation results demonstrate that the DentalTouch prototype has the maximum measured stiffness up to 69 N/mm and low inertia ranging from 113 g to 163 g. These results suggest that the DentalTouch has a potential to provide both high stiffness and low inertia.

We showed that the DentalTouch is able to render rigid constraints when the device mechanism makes contact with the physical constraints of the co-actuation modules. However, this rigid constraint is unilateral. To render bilateral rigid constraints, switching from one contact direction to the opposite contact direction may result in a short period of low impedance state, which may be perceived by the operator. Further study is necessary to explore how this effect

influences the simulation performance of the device.

The stiffness value obtained in this paper is limited to the structural and motor control stiffness. Future work is planned to fully explore the potential of the DentalTouch in providing both high stiffness and low inertia.

APPENDIX

A. Jacobian matrix

The Jacobian matrix J of the DentalTouch can be deduced by the procedure synthetically reported in the following.

The kinematics of the 3R limb is given by [20]:

$$X = f(\theta_3, \theta_4, \theta_5) \qquad (1\text{-A})$$

where X is the position vector of the point Q.

By formulating the derivative of Eq. (1-A), we have

$$\dot{X} = R\,\dot{\Theta}_1 \qquad (2\text{-A})$$

where $\dot{X} = [\dot{x}\quad \dot{y}\quad \dot{z}]^T$ and $\dot{\Theta}_1 = \begin{bmatrix}\dot{\theta}_3 & \dot{\theta}_4 & \dot{\theta}_5\end{bmatrix}^T$.

Two following constraint equations can be obtained as [20]:

$$\begin{cases} L_2^2 = |BC|^2 \\ L_4^2 = |EF|^2 \end{cases} \qquad (3\text{-A})$$

Taking derivative of Eq. (3-A) yields the following expression

$$\begin{cases} 0 = f\dot{\theta}_3 + g\dot{\theta}_4 + h\dot{\theta}_5 + p\dot{\theta}_1 \\ 0 = l\dot{\theta}_3 + m\dot{\theta}_4 + n\dot{\theta}_5 + q\dot{\theta}_2 \end{cases} \qquad (4\text{-A})$$

where

$$f = \frac{\partial f_1}{\partial \theta_3}, g = \frac{\partial f_1}{\partial \theta_4}, h = \frac{\partial f_1}{\partial \theta_5}, p = \frac{\partial f_1}{\partial \theta_1}$$

$$l = \frac{\partial f_2}{\partial \theta_3}, m = \frac{\partial f_2}{\partial \theta_4}, n = \frac{\partial f_2}{\partial \theta_5}, q = \frac{\partial f_2}{\partial \theta_2} \qquad (5\text{-A})$$

f_1 and f_2 represent the expression of the right hand side of Eq. (3-A).

Solving Eq. (4-A) for $\dot{\theta}_4$ and $\dot{\theta}_5$, we obtain

$$\dot{\theta}_4 = [(hl - nf)\dot{\theta}_3 + hq\dot{\theta}_2 - np\dot{\theta}_1]/(gn - mh)$$
$$\dot{\theta}_5 = [(mf - gl)\dot{\theta}_3 - gq\dot{\theta}_2 + mp\dot{\theta}_1]/(gn - mh) \qquad (6\text{-A})$$

Substituting (6-A) into (2-A), we get the expression of the Jacobian matrix J, the elements of which are as follows (i=1 to 3):

$$J_{i1} = r_{i1} + \frac{hl - nf}{gn - mh}r_{i2} + \frac{mf - gl}{gn - mh}r_{i3}$$

$$J_{i2} = \frac{hq}{gn - mh}r_{i2} - \frac{gq}{gn - mh}r_{i3} \qquad (7\text{-A})$$

$$J_{i3} = \frac{-np}{gn - mh}r_{i2} + \frac{mp}{gn - mh}r_{i3}$$

B. Effective gravity

The effective gravity of the end-effector, G_e, can be expressed as:

$$G_e = \sum_{i=1}^{6} G_i \qquad (8\text{-}A)$$

where

$$G_1 = \lambda_1 m_1 g L_1 s\theta_1 J_{13}^{-1}$$
$$G_2 = \lambda_2 m_2 g L_3 s\theta_2 J_{23}^{-1}$$
$$G_3 = \lambda_3 m_3 g L_5 s\theta_3 J_{33}^{-1} \qquad (9\text{-}A)$$
$$G_4 = (1-\lambda_4) m_3 g L_5 s\theta_3 J_{33}^{-1} + \lambda_4 m_4 g$$
$$G_5 = (1-\lambda_5) m_5 g L_1 s\theta_1 J_{13}^{-1} + p\lambda_5 m_5 g$$
$$G_6 = (1-\lambda_6) m_6 g L_3 s\theta_2 J_{23}^{-1} + q\lambda_6 m_6 g$$

and m_i (i=1 to 6) are mass of links including *AB, DE, MN, BC, EF* and the moving platform. λ_i (i=1 to 6) are constants which define the centroids of the links. J_{ij}^{-1} is the ijth element of J^{-1} (i, j=1 to 3). p and q are expressed as:

$$p = L_5 s\theta_3 R_{13}^{-1} + dc\theta_5 c(\theta_3 + \theta_4) R_{33}^{-1} - ds\theta_5 s(\theta_3 + \theta_4)(R_{23}^{-1} + R_{33}^{-1})$$
$$- L_6 c\theta_5 s(\theta_3 + \theta_4)(R_{13}^{-1} + R_{23}^{-1}) - L_6 s\theta_5 c(\theta_4 + \theta_5) R_{33}^{-1}$$

$$q = -L_5 s\theta_3 R_{13}^{-1} - dc\theta_5 c(\theta_3 + \theta_4) R_{33}^{-1} + ds\theta_5 s(\theta_3 + \theta_4)(R_{23}^{-1} + R_{33}^{-1})$$
$$- L_6 c\theta_5 s(\theta_3 + \theta_4)(R_{13}^{-1} + R_{23}^{-1}) - L_6 s\theta_5 c(\theta_4 + \theta_5) R_{33}^{-1}$$

$$(10\text{-}A)$$

where R is defined in Eq. (2-A) and R_{ij}^{-1} is the ijth element of R^{-1} (i, j=1 to 3).

ACKNOWLEDGMENT

REFERENCES

[1] D. Wang, Y. Zhang, J. Hou, *et al*, "iDental: a haptic-based dental simulator and its preliminary evaluation," *IEEE Trans. Haptics*, vol. 5, no. 4, pp. 332-343, 2012.

[2] H. Tan, B. Eberman, M. Srinivasan, and B. Cheng, "Human factors for the design of force-reflecting haptic interfaces," in *ASME DSC*, vol. 55, no. 1, Chicago, IL, 1994, pp. 353–359.

[3] T. Massie, J. Salisbury, "The PHANTOM haptic interface: a device for probing virtual objects," in *ASME Winter Annual Meeting*, Symposium on Haptic Interfaces for Virtual Environment and Teleoperator Systems, vol. DSC 55, Chicago, IL, 1994, pp. 295–302.

[4] K. Salisbury, B. Eberman, M. Levin, W. Townsend, "The design and control of an experimental whole-arm manipulator," in *The Fifth International Symposium on Robotics Research*, 1990, pp. 233-241.

[5] R. Van der Linde, P. Lammertse, E. Frederiksen, B. Ruiter, "The haptic master, a new high-performance haptic interface," in *Proceedings of Euro-Haptics*, Edinburgh, U.K., 2002, pp. 1-5.

[6] E. Faulring, J. Colgate, M. Peshkin, "The cobotic hand controller: design, control and performance of a novel haptic display," *Int. J. Robot. Res.*, vol. 25, no. 11, pp. 1099-1119, 2005.

[7] http://www.geomagic.com/en/products-landing-pages/haptic.

[8] M. Zinn, O. Khatib, B. Roth, J. K. Salisbury, "Large workspace haptic devices: a new actuation approach," in *Symposium on Haptic Interfaces for Virtual Environment and Teleoperator Systems*, 2008, pp. 185-192.

[9] C. Cho, J. B. Song, M. Kim, "Energy-based control of a haptic device using brakes," *IEEE Trans. Syst. Man. Cybern*, vol. 37, no. 2, pp. 341-349, 2007.

[10] F. Conti, O. Khatib, C. Baur, "A hybrid actuation approach for haptic devices," in *World Haptics*, 2007, pp. 367-372.

[11] J. An, D. S. Kwon, "Stability and performance of haptic interfaces with active/passive actuators theory and experiments," *Int. J. Robot. Res.* vol. 25, no. 11, pp. 1121-1136, 2006.

[12] T. B. Kwon, J. B. Song, "Force display using a hybrid haptic device composed of motors and brakes," *Mechatronics*, vol. 16, 249-257, 2006.

[13] D. K. Swanson, W. J. Book, "Path-following control for dissipative passive haptic displays," in *Proceedings of the 11th Symposium on Haptic Interfaces for Virtual Environment and Teleoperator Systems*, March 2003, pp. 101-108.

[14] A. Gosline, V. Hayward, "Eddy current brakes for haptic interfaces: design, identification, and control," *IEEE/ASME Trans. Mechatron.*, vol. 13, no. 6, pp. 669-677, 2008.

[15] D. W. Weir, J. E. Colgate, M. A. Peshkin, "Measuring and increasing Z-width with active electrical damping," in *Proceedings of the Symposium on Haptic Interfaces for Virtual Environment and Teleoperator Systems*, 2008, pp. 169-175, 2008.

[16] N. Hungr, B. Roger, A. J. Hodgson, C. Plaskos, "Dynamic physical constraints: emulating hard surfaces with high realism," *IEEE Trans. Haptics*, vol. 5, no. 1, pp. 48-57, 2012.

[17] D. Wang, Y. Zhang, T. Li, *et al.*, "Survey on multisensory feedback virtual reality dental training systems," *European Journal of Dental Education*, vol. 20, no. 4, pp. 248-260, 2015.

[18] P. Lammertse, "Haptic User Interface," U.S. Patent 8 716 973 B1, February 28, 2012.

[19] J. Song, Y. Zhang, H. Zhang, *et al*, "Co-actuation: achieve high stiffness and low inertia in force feedback device," in *Proceedings of Euro-Haptics*, London, UK, 2016, pp. 229-239.

[20] H. Zhang, Y. Zhang, and D. Wang, "Real-Time Solutions to the Forward Kinematics of a 2RSS+RRR Parallel Mechanism," *Mechanism and Machine Science*, vol. 408, pp.995-1008, 2017.

[21] D. Checcacci, E. Sotgiu, A. Frisoli, *et al*, "Gravity compensation algorithms for parallel haptic interface," in *Proceeding of the IEEE Intelnational Workshop on Robot and Human Interactive Communication*, Germany, 2002, pp. 140-145.

[22] John J. Craig, *Introduction to robotic: Mechanics and Control*. USA: Pearson Prentice Hall, 2005. Ch. 6.

[23] B. Monsarrat, C. M. Gosselin, "Workspace analysis and optimal design of a 3-leg 6-DOF parallel platform mechanism," *IEEE Transaction on Robotics and Automation*, vol. 19, no. 6, pp. 954-967, 2003.

[24] C. M. Gosselin, J. Wang, T. Laliberté, and I. Ebert-Uphoff, "On the design of a statically balanced 6-DOF parallel manipulator," in *Proc. IFToMM 10th World Congr. Theory of Machines and Mechanisms*, Oulu, Finland, pp. 1045-1050, 1999.